Simulation study on cascaded terahertz pulse generation in electro-optic crystals

Simulation study on cascaded terahertz pulse generation in electro-optic crystals

Toshiaki Hattori and Kousuke Takeuchi

Institute of Applied Physics, University of Tsukuba, 1-1-1 Tennodai, Tsukuba, Ibaraki 305-8573, Japan

hattori@bk.tsukuba.ac.jp

Abstract: We studied cascaded optical rectification processes for intense terahertz (THz) pulse generation in electro-optic crystals using simulations based on one-dimensional coupled propagation equations of THz and optical fields. We found that under ideal conditions of perfect phase matching and no absorption, cascaded optical rectification processes produce intense THz pulses with efficiencies exceeding the Manley-Rowe limit. Large red shifting of the pump light spectrum was observed. Effects of finite optical and THz absorption, phase mismatches, and pulse width were examined using parameters of a ZnTe crystal pumped by 800 nm pulses. THz field enhancement by multiple pulse pumping was also studied.

© 2007 Optical Society of America

OCIS codes: (190.2620) Frequency conversion; (190.7110) Ultrafast nonlinear optics; (260.3090) Physical optics, Infrared, far; (000.4430) Numerical approximation and analysis.

References and links

1. B. Ferguson, and X. -C. Zhang, "Materials for terahertz science and technology," Nature Materials **1,** 26-33 (2002).
2. B. B. Hu and M. C. Nuss, "Imaging with terahertz waves," Opt. Lett. **20,** 1716–1718 (1995).
3. R. Rungsawang, A. Mochiduki, S. Ookuma, and T. Hattori, "1-kHz real-time imaging using a half-cycle terahertz electromagnetic pulse," Jpn. J. Appl. Phys. **44,** L288–L291 (2005).
4. D. J. Cook, J. X. Chen, E. A. Morlino, and R. M. Hochstrasser, "Terahertz-field-induced second-harmonic generation measurements of liquid dynamics," Chem. Phys. Lett. **309,** 221–228 (1999).
5. C. Luo, K. Reimann, M. Woerner, and T. Elsaesser, "Nonlinear terahertz spectroscopy of semiconductor nanostructures," Appl. Phys. A **78,** 435–440 (2004).
6. T. Löffler, M. Kreß, M. Thomson, T. Hahn, N. Hasegawa, and H. G. Roskos, "Comparative performance of terahertz emitters in amplifier-laser-based systems," Semicond. Sci. Technol. **20,** S134–141 (2005).
7. D. You, R. R. Jones, P. H. Bucksbaum, and D. R. Dykaar, "Generation of high-power sub-single-cycle 500-fs electromagnetic pulses," Opt. Lett. **18,** 290–292 (1993).
8. E. Budiarto, J. Margolies, S. Jeong, J. Son, and J. Bokor, "High-intensity terahertz pulses at 1-kHz repetition rate," IEEE J. Quantum Electron. **32,** 1839–1846 (1996).
9. T. Hattori, K. Tukamoto, and H. Nakatsuka, "Time-resolved study of intense terahertz pulses generated by a large-aperture photoconductive antenna," Jpn. J. Appl. Phys. **40,** 4907–4912 (2001).
10. T. Hattori, K. Egawa, S. Ookuma, and T. Itatani, "Intense terahertz pulses from large-aperture antenna with interdigitated electrodes," Jpn. J. Appl. Phys. **45,** L422–L424 (2006).
11. T. J. Carrig, G. Rodriguez, T. S. Clement, A. J. Taylor, and K. R. Stewart, "Generation of terahertz radiation using electro-optic crystal mosaics," Appl. Phys. Lett. **66,** 10–12 (1995).
12. K. Reimann, R. P. Smith, A. M. Weiner, T. Elsaesser, and M. Woerner, "Direct field-resolved deetction of terahertz transients with amplitudes of megavolts per centimeter," Opt. Lett. **28,** 471–473 (2003).
13. T. Löffler, T. Hahn, M. Thomson, F. Jacob, and H. G. Roskos, "Large-area electro-optic ZnTe terahertz emitters," Opt. Express **13,** 5353–5362 (2005).
14. F. G. Sun, W. Ji, and X. -C. Zhang, "Two-photon absorption induced saturation of THz radiation in ZnTe," in Conference on Lasers and Electro-Optics, OSA Technichal Digest (Optical Society of America, Wasgington DC, 2000), 479–480.

15. M. Nagai, K. Tanaka, H. Ohtake, T. Bessho, T. Sugiura, T. Hirosumi, and M. Yoshida, "Generation and detection of terahertz radiation by electro-optic process in GaAs using 1.56 μm fiber laser pulses," Appl. Phys. Lett. **85,** 3974–3976 (2004).
16. G. Gallot, J. Zhang, R. W. McGowan, T. -I. Jeon, and D. Grischkowsky, "Measurements of the THz absorption and dispersion of ZnTe and their relevance to the electro-optic detection of THz radiation," Appl. Phys. Lett. **74** 3450-3452 (1999).
17. M. Schall and P. Uhd. Jepsen, "Freeze-out of difference-phonon modes in ZnTe and its application in detection of THz pulses," Appl. Phys. Lett. **77,** 2801–2803 (2000).
18. M. Schall, M. Walther, and P. Uhd. Jepsen, "Fundamental and second-order phonon processes in CdTe and ZnTe," Phys. Rev. B **64,** 094301 (2001).
19. K. L. Vodopyanov, "Optical generation of narrow-band terahertz packets in periodically-inverted electro-optic crystals: conversion efficiency and optimal laser pulse format," Opt. Express **14,** 2263–2276 (2006).
20. J. Hebling, A. G. Stepanov, G. Almási, B. Bartal and J. Kuhl, "Tunable THz pulse generation by optical rectification of ultrashort laser pulses with tilted pulse fronts," Appl. Phys. B **78,** 593–599 (2004).
21. A. G. Stepanov, J. Kuhl, I. Z. Kozma, E. Riedle, G. Almási, and J. Hebling, "Scaling up the energy of THz pulses created by optical rectification," Opt. Express **13,** 5762–5768 (2005).
22. R. W. Boyd, *Nonlinear Optics* (Academic, San Diego, 2003).
23. M. Cronin-Golomb, "Cascaded nonlinear difference-frequency generation of enhanced terahertz wave generation," Opt. Lett. **29,** 2046–2048 (2004).
24. J. M. Fraser and C. Ventalon, "Parametric cascade downconverter for intense ultrafast mid-infrared generation beyond the Maley-Rowe limit," Appl. Opt. **45,** 4109–4113 (2006).
25. Ch. Bosshard, R. Spreiter, M. Zgonik, and P. Günter, "Kerr nonlinearity via cascaded optical rectification and the linear electro-optic effect," Phys. Rev. Lett. **74,** 2816–2819 (1995).
26. J. -P. Caumes, L. Videau, C. Rouyer, and E. Freysz, "Ker-like nonlinearity induced via terahertz generation and the electro-optical effect in zinc blende crystals," Phys. Rev. Lett. **89,** 047401 (2002).
27. C. Kolleck, "Cascaded second-order contribution to the third-order nonlinear susceptibility," Phys. Rev. A **69,** 053812 (2004).
28. W. -Q. He, C. -M. Gu, and W. -Z. Shen, "Direct evidence of Kerr-like nonlinearity by femtosecond Z-scan technique," Opt. Express **14,** 5476–5483 (2006).
29. S. Casalbuoni, H. Schlarb, B. Schmidt, P. Schmüser, B. Steffen, and A. Winter, "Numerical studies on the electro-optic sampling of relativistic electron bubches," TESLA Report 2005-11 (2005).
30. A. Nahata, A. S. Weling, and T. F. Heinz, "A wideband coherent terahertz spectroscopy system using optical rectification and electro-optic sampling," Appl. Phys. Lett. **69,** 2321–2323 (1996).
31. R. E. Nahory and H. Y. Fan, "Optical properties of zinc telluride," Phys. Rev. **156,** 825–833 (1967).

---

1. Introduction

Terahertz (THz) pulses can be used in many applications in security inspections, spectroscopies, and other fields[1]. Generation of intense THz pulses is required for real-time measurements[2, 3] and investigation of nonlinear phenomena[4, 5]. Two types of apparatuses have been widely used in laboratory based systems for intense THz pulse generation[6]. One is a large-aperture photoconductive antenna[7, 8, 9, 10], and the other used optical rectification (OR) processes in electro-optic (EO) crystals[11, 12, 13]. Advantages of the use of EO crystals are broad bandwidth of emitted THz waves, high saturation fluence of the pump light, and scalability. THz pulse intensity scaling using a large area mosaic of EO crystals has been reported[11].

Saturation of THz intensity under large pump light fluence have been observed in ZnTe crystals and attributed to two-photon absorption[13, 14]. Loss of the pump light energy due to two-photon absorption and absorption of THz waves by the carriers generated by the two-photon absorption can limit the achievable level of THz intensity. Possible solution for this problem is lowering the two-photon absorption cross-section using other crystals[15]. Other reported methods to obtain intense THz pulses using EO crystals are based on reduction of absorption by lowering the temperature of the crystal[16, 17, 18] or shaping the pump pulses[19]. Recently, a method to achieve phase matching using tilted pulse fronts has been applied to THz pulse generation in lithium niobate and succeded in generating THz pulses of μJ level[20, 21].

Under almost perfect phase matching conditions, more fundamental question arises: *i.e.*,

what limits the conversion efficiency. Influence of pump light depletion on the THz generation efficiency is of general and practical interest. Since THz wave generation by OR is a difference frequency generation (DFG) process between optical fields within the pump light spectrum, photon number of the pump light does not change during the THz generation although the spectrum is expected to be shifted to lower frequencies. Manley-Rowe relation[22] for nonlinear optical mixing states that one difference-frequency photon is created via annihilation of one pump photon. This relation leads to the Manley-Rowe limit of conversion efficiency that the emitted photon number of the difference frequency field cannot exceed the photon number of the pump light. Since THz photon energy is about two orders of magnitude smaller than optical photon energy, energy conversion efficiency of less than 1% at maximum is expected. In the OR process, however, the red-shifted pump photon can be reused for the generation of a second THz photon, and the cascaded OR processes can give conversion efficiency much higher than the Manley-Rowe limit[19]. For DFG of two narrow band light fields, possibility of achieving high conversion efficiency using cascaded DFG processes has been analyzed[23, 24].

To investigate the effects of cascading, we conducted numerical simulations using coupled equations of propagation of the pump and THz fields. Simulations were performed based on one-dimensional propagation equations using parameters of a ZnTe crystal pumped by 800 nm femtosecond optical pulses. The purpose of this paper is twofold. One is to study the features of the behaviors of the optical and THz field when cascaded OR occurs to a significant extent. For this perpose, ideal case was studied where the phase matching is perfect and there is no absorption. The other purpose is to search for the optimal condition for generation of the largest THz wave output. For this perpose, more realistic parameters of ZnTe were used. Effects of phase matching and linear absorption was studied and the results were compared with those of ideal conditions free from phase mismatch and absorption. Effects of pump pulse width and multiple pulse pumping were also studied, which can lower the two-photon absorption and narrow the THz wave spectrum. Third-order Kerr-like nonlinearity via cascaded OR processes in EO media has been studied[25, 26, 27, 28]. This type of nonlinearity is automatically included in the present simulations. Time dependent refractive index change generally induces spectrum modification to ultrashort optical pulses. The spectrum changes of the pump light observed in this study, therefore, include third-order and higher-order effects. On the other hand, two-photon absorption, which is another type of direct third-order nonlinearity, was not included in the simulation model explicitly.

2. Theoretical model

2.1. Material parameters

We use parameters of ZnTe for the EO medium. Since Ti:sapphire laser based amplifier systems are almost the only solution for intense femotosecond pulses although high power fiber laser amplifier systems are being developed recently, we set the pump wavelength at 800 nm. Dispersion of ZnTe in THz region is described by a dielectric function at frequency v:

$$\varepsilon(v) = \varepsilon_{\mathrm{el}} + \frac{S_0 v_0^2}{v_0^2 - v^2 - i\Gamma_0 v},$$ (1)

with $\varepsilon_{\mathrm{el}} = 7.44$, $v_0 = 5.32$ THz, $\Gamma_0 = 0.09$ THz, and $S_0 = 2.58$, as reported by Gallot *et al.* [16, 29]. For the optical region, we used a Sellmeier equation for refractive index $n(\lambda)$[30]:

$$n(\lambda) = \left(4.27 + \frac{3.01\lambda^2}{\lambda^2 - 0.142}\right)^{1/2}.$$ (2)

Here, λ is the wavelength in μm. Refractive index in the THz and optical regions is plotted as a function of frequency in Fig. 1. When group velocity dispersion is neglected within the pump
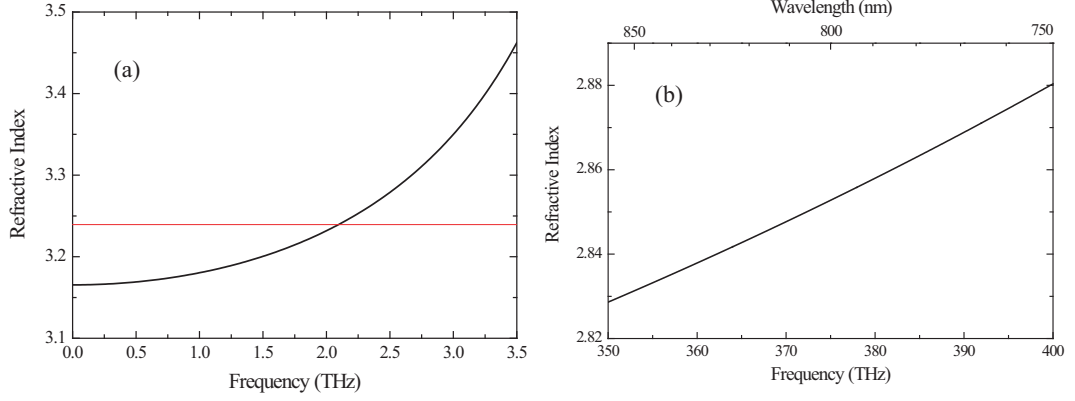
Fig. 1. Dispersion relation of ZnTe in the (a) THz and (b) optical regions. Red horizontal
line in (a) shows the group refractive index at 375 THz (*i.e.*, 800 nm).

light spectrum, the phase matching condition for the OR process is expressed as[30]

$$n(\omega_T) = n_g(\omega_{\text{opt}}), \tag{3}$$

where ω_T is the THz ferquency and $n_g(\omega_{\text{opt}})$ is the group refractive index at optical frquencies.
In Fig. 1(a) is shown the group refractive index at 800 nm by a red horizontal line. The phase
matching condition is satisfied at THz wave frequency of 2.1 THz. For the simulations under
perfect phase matching conditions, the THz refractive index was set constant at the values of
this frequency.

Absorption in the THz region that is not included in the THz dispersion relation of Eq. (1)
has been reported[16, 18]. We used $\alpha_T = 12\ \text{cm}^{-1}$ for the absorption coefficient for THz waves.
We set it as a constant independent of frequency for simplicity of calculations. Since this value
approximately corresponds to the maximum absorption coefficient in the frequency region be-
low 2.5 THz, it may be an overestimate. The strong absorption in the phonon resonance region
around 5.3 THz was not taken into account. Thus we used only data below 5.3 THz because we
found spurious results in the resonance region in some cases because of strong dispersion. The
absorption coefficient for optical waves was set as $\alpha_L = 3\ \text{cm}^{-1}$[23, 31].

When a (110) ZnTe crystal is used for the THz wave generation, the amplitude of the THz
wave becomes maximum when the incident light polarization lies in $[\bar{1}, 1, 1]$ direction. Further-
more, it is the case when the polarization of the optical field generated by the cascaded mixing
of the incident light and the THz field becomes parallel to the incident polarization so that
cascading can continue further. Consequently, we set the incident light polarization in this di-
rection. The THz wave polarization is also in the same direction. The effective nonlinear optical
coefficient d_{eff} in this configuration is related to the tensor element d_{14} as

$$d_{\text{eff}} = \frac{2}{\sqrt{3}} d_{14}. \tag{4}$$

We derived the value of d_{14} for the simulations using the reported electro-optic constant r_{41} as

$$d_{14} = -\frac{\varepsilon_0 n_o^4 r_{41}}{2}, \tag{5}$$

where ε_0 is the vacuum dielectric constant, n_0 is the refractive index of light at the center wave-
length, and $r_{41} = 3.9\ \text{pm/V}$[29], which yields $d_{14}/\varepsilon_0 = 129\ \text{pm/V}$. We set the nonlinear optical
coefficient as constant and neglected the dispersion since our simulations do not deal with the
phonon resonance region, where large dispersion exists in the nonlinear optical coefficient.

2.2. Propagation equations

One-dimensional coupled wave equations of the optical and THz waves were derived using the wave equation[22]:

$$\frac{\partial^2 E(z,t)}{\partial z^2} - \varepsilon\mu\frac{\partial^2 E(z,t)}{\partial t^2} - \mu\sigma\frac{\partial E(z,t)}{\partial t} = \mu\frac{\partial^2 P(z,t)}{\partial t^2}. \tag{6}$$

Here,

$$E(z,t) = E_L(z,t) + E_T(z,t) \tag{7}$$

is the electric field composed of an optical frequency component, $E_L(z,t)$, and a THz frequency component, $E_T(z,t)$, ε is the dielectric constant, μ is the magnetic permeability, which is assumed to be that of vacuum and independent of frequency, σ is the conductivity, which is related to the absorption coefficient, and

$$P(z,t) = 2d_{\text{eff}}[E(z,t)]^2 \tag{8}$$

is the nonlinear polarization composed of optical and THz components. Both optical and THz waves are assumed to propagate in z direction.

The electric fields of the pump light are expressed using a slowly varying envelope $e_L(z,t)$ as

$$E_L(z,t) = \frac{1}{2}e_L(z,t)\exp(-i\omega_0 t) + \text{c.c.}, \tag{9}$$

where ω_0 is the center frequency of the light spectrum. Envelope $e_L(z,t)$ is expressed in terms of Fourier components as

$$e_L(z,t) = \int E_L(z,\omega)\exp[ik(\omega+\omega_0)z - i\omega t]\,d\omega. \tag{10}$$

The THz waves are expressed as

$$E_T(z,t) = \int E_T(z,\omega_T)\exp[ik(\omega_T)z - i\omega_T t]\,d\omega_T. \tag{11}$$

Here, $k(\omega+\omega_0)$ and $k(\omega_T)$ are the real wavevectors at respective frequencies, which are determined by the dispersion relation. The integration for the optical waves is carried out over positive frequencies of the spectrum of the light. The THz Fourier component, on the other hand, is set to be centered at zero frequency, and the integration is performed over positive and negative frequencies.

Under the slowly-varying envelope approximation, the one-dimensional coupled propagation equations are derived as

$$\frac{\partial}{\partial z}E_L(z,\omega) = -\frac{\alpha_L}{2}E_L(z,\omega)$$
$$+ i\frac{2\mu d_{\text{eff}}(\omega+\omega_0)^2}{k(\omega+\omega_0)}\int E_L(z,\omega-\omega_T)E_T(z,\omega_T)\exp(i\Delta k_L z)d\omega_T, \tag{12}$$

$$\frac{\partial}{\partial z}E_T(z,\omega_T) = -\frac{\alpha_T}{2}E_T(z,\omega_T) + i\frac{\mu d_{\text{eff}}\omega_T^2}{2k(\omega_T)}\int E_L(z,\omega+\omega_T)E_L^*(z,\omega)\exp(i\Delta k_T z)d\omega. \tag{13}$$

Here, Δk_L and Δk_T are phase mismatches defined by

$$\Delta k_L \equiv k(\omega+\omega_0-\omega_T) + k(\omega_T) - k(\omega+\omega_0), \tag{14}$$

$$\Delta k_T \equiv k(\omega + \omega_0 + \omega_T) - k(\omega + \omega_0) - k(\omega_T). \tag{15}$$

The first term in Eq. (12) describes the effects of linear absorption and the second term that of sum-frequency (for $\omega_T > 0$) and difference-frequency (for $\omega_T < 0$) generation between the optical and THz photons on the propagation of the optical field. The first term in Eq. (13) describes the effects of linear absorption and the second term that of difference-frequency generation between two optical photons on the propagation of the THz field. Effects of nonlinear mixing between THz photons were omitted since they are weaker by a factor of ω_T/ω_0 even if the THz field grows to an amplitude comparable with that of the optical field. In simulations for perfect phase matching conditions, these phase mismatches were set zero. Simulations for the lossless case and for a realistic absorption case were conducted. For the lossless case we set $\alpha_L = \alpha_T = 0$.

2.3. Analytical expressions

When the pump light is weak and effects of cascading can be neglected, we can drop the second term in the right hand side of Eq. (12), and obtain the THz field as

$$E_T(z, \omega_T) = i \frac{\mu d_{\text{eff}} \omega_T^2}{2k(\omega_T)} \int d\omega\, E_L(\omega + \omega_T) E_L^*(\omega) \frac{e^{(i\Delta k_T - \alpha_L)z} - e^{-\alpha_T z/2}}{(\alpha_T/2) - \alpha_L + i\Delta k_T}, \tag{16}$$

where $E_T(z = 0, \omega_T) = 0$ is assumed, and $E_L(\omega) \equiv E_L(z = 0, \omega)$ is the incident light spectrum. When further assuming that the phase matching is perfect and there are no losses, this equation becomes simply

$$\begin{aligned} E_T(z, \omega_T) &= i \frac{\mu d_{\text{eff}} \omega_T^2 z}{2k(\omega_T)} \int d\omega\, E_L(\omega + \omega_T) E_L^*(\omega) \\ &= i \frac{\mu c d_{\text{eff}} \omega_T z}{2n_T(\omega_T)} \int d\omega\, E_L(\omega + \omega_T) E_L^*(\omega), \end{aligned} \tag{17}$$

where $n_T(\omega_T)$ is the refractive index at a THz frequency ω_T. When we neglect the dispersion in the THz frequencies, Eq. (17) leads to a simpler expression in time domain,

$$E_T(z, t) = -\frac{\mu c d_{\text{eff}} z}{2n_T} \cdot \frac{\partial}{\partial t} |e_L(t)|^2, \tag{18}$$

which is helpful to get basic physical insight of the processes under consideration. Here, c is the speed of light in vacuum.

In the simulation, the incident light pulses were assumed to have a Gaussian temporal shape as

$$e_L(0, t) = E_0 \exp\left(-2\ln 2 \frac{t^2}{\delta t^2}\right), \tag{19}$$

where δt is the pulse width, which is defined by the full width at half maximum of the intensity pulse shape. The Fourier transform of the incident optical wave becomes

$$E_L(0, \omega) = \frac{E_0 \delta t}{2\sqrt{2\pi \ln 2}} \exp\left(-\frac{\delta t^2}{8\ln 2} \omega^2\right). \tag{20}$$

The energy conversion efficiency, r_E, and photon conversion ratio, r_p, from optical to THz waves are expressed as

$$r_E = 2 \int |E_T(z, \omega_T)|^2 d\omega_T \Big/ \int |E_L(0, \omega)|^2 d\omega, \tag{21}$$

$$r_p = 2 \int \frac{|E_T(z, \omega_T)|^2}{|\omega_T|} d\omega_T \bigg/ \int \frac{|E_L(0, \omega)|^2}{|\omega + \omega_0|} d\omega. \tag{22}$$

Now we derive the propagation distance, r_c, where the photon conversion ratio reaches unity under the ideal case of perfect phase matching and no losses, using Eq. (17). This length, which we refer to a "cascading length," is a measure of the magnitude of the nonlinear interaction. By assuming a Gaussian pulse shape as given in Eq. (19), we obtain

$$E_T(z, \omega_T) = i \frac{\mu d_{\text{eff}} c \delta t \, \omega_T}{8 \sqrt{\pi \ln 2} \, n_T(\omega_T)} E_0^2 z \exp\left(-\frac{\delta t^2}{16 \ln 2} \omega_T^2\right), \tag{23}$$

and the numerator of Eq. (22) becomes

$$2 \int \frac{|E_T(z, \omega_T)|^2}{|\omega_T|} d\omega_T = \frac{1}{4\pi} \left(\frac{\mu d_{\text{eff}} c}{n_T} E_0^2 z\right)^2, \tag{24}$$

when the dispersion in THz region is neglected. The denominator of Eq. (22), on the other hand, is

$$\int_{-\infty}^{\infty} \frac{|E_L(0, \omega)|^2}{|\omega + \omega_0|} d\omega = \frac{\delta t^2}{8\pi \ln 2} E_0^2 \int_{-\infty}^{\infty} \frac{1}{|\omega + \omega_0|} \exp\left(-\frac{\delta t^2}{4 \ln 2} \omega^2\right) d\omega$$

$$= \frac{\delta t}{4 \sqrt{\pi \ln 2} \, \omega_0} E_0^2. \tag{25}$$

Here, the approximation

$$\omega + \omega_0 \simeq \omega_0 \tag{26}$$

is used since the spectrum width is much narrower than the center frequency. Equations (24) and (25) lead to the propagation distance z_c where the condition of $r_p = 1$ is satisfied as

$$z_c = \frac{n_T}{\mu d_{\text{eff}} c E_0} \sqrt{\frac{\delta t}{\omega_0}} \sqrt{\frac{\pi}{\ln 2}}. \tag{27}$$

For analytical evaluation of the effects of absorption, we define an absorption length, z_a, as the propagation distance where the THz field becomes maximum when under perfect phase matching and no losses. Using Eq. (16), we obtain

$$z_a = \frac{1}{(\alpha_T/2) - \alpha_L} \ln\left(\frac{\alpha_T}{2\alpha_L}\right). \tag{28}$$

3. Simulation results

Numerical integrations of Eqs. (12) and (13) were conducted using the Runge-Kutta method with a step of 0.01 mm.

3.1. $\Delta k = 0$, $\alpha = 0$ case

First we conducted numerical calculations under conditions of perfect phase matching ($\Delta k_L = \Delta k_T = 0$) and no absorption ($\alpha_T = \alpha_L = 0$) in order to understand the basic physical nature of the cascaded OR processes. When ZnTe is used as the EO medium, perfect phase matching is achieved only around 2 THz. Since the linear optical properties of ZnTe are isotropic, phase matching condition cannot be controlled by changing the orientation of the crystal. Broadband
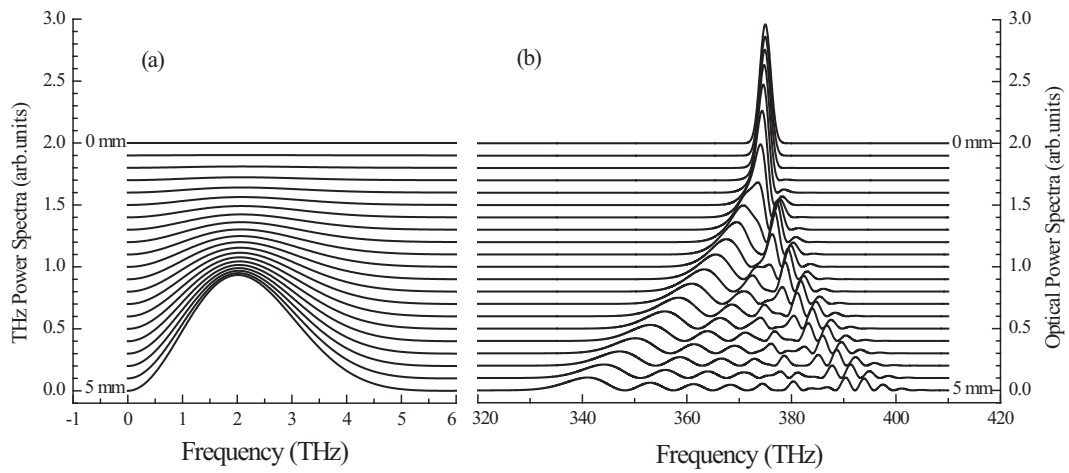
Fig. 2. Power spectra of (a) THz and (b) optical fields under perfect phase matching and no absorption conditions at propagation distances in the ZnTe crystal from 0 to 5 mm by a step of 0.25 mm. Each spectrum is shifted upward by 0.1.
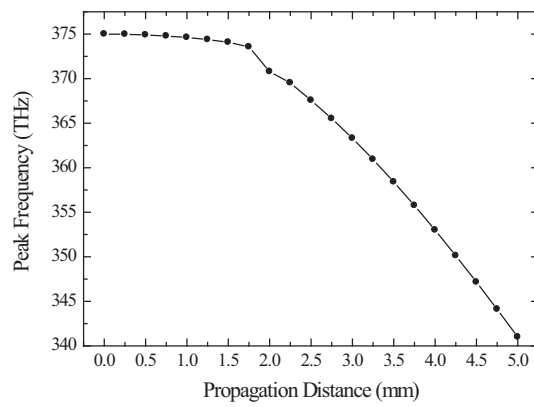

Fig. 3. Peak frequency of the optical spectrum as a function of propagation distance obtained under perfect phase matching and no absorption conditions.
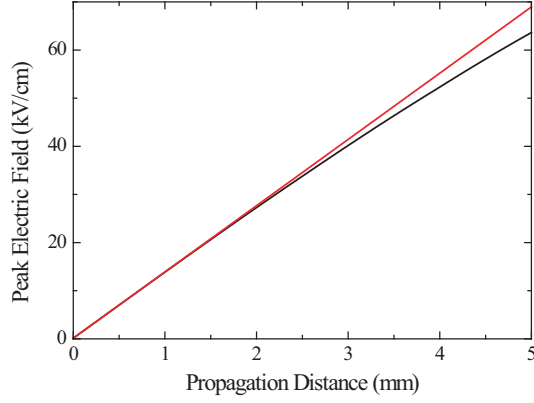
Fig. 4. Black line shows peak field of THz pulses in time domain as a function of propagation distance under perfect phase matching and no absorption conditions. Red line is a straight line that is obtained assuming no pump light change.
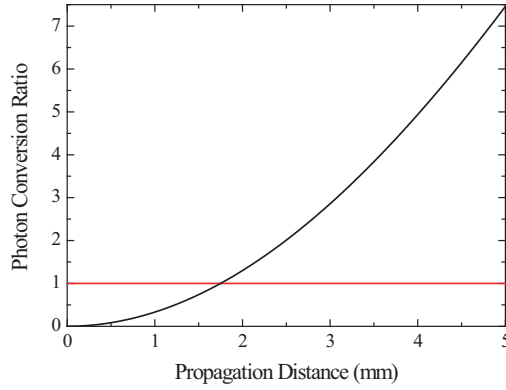
Fig. 5. Photon conversion ratio from optical to THz photons under perfect phase matching and no absorption conditions. Red line shows the level of unity, which corresponds to the Manley-Rowe limit.

phase matching, however, can be achieved by using other EO media such as $LiNbO_3$ and applying, if necessary, the tilted pulse front method. The aim of the simulations described in this subsection, therefore, is to understand the ideal case.

It was assumed that the incident pump light pulse has a Gaussian temporal shape of 180 fs duration and peak intensity of 300 MW/cm^2, which corresponds to a pump fluence of 57 μJ/cm^2. The cascading length, z_c, as defined by Eq. (27) is 1.76 mm at this incident fluence.

Power spectra of THz and optical waves obtained by the calculation are shown in Fig. 2 as a function of propagation distance in ZnTe from 0 to 5 mm. The THz spectra grows almost linearly as a function of propagation distance, and little change in the shape is observed. On the other hand, the optical spectra show red shifting and the speed of the shift becomes faster as the pump pulse propagates.

We plot the frequency of the peak of the optical spectra as a function propagatin distance in Fig. 3. The red shifting of the optical spectra shows quadratic dependence on the propagation distance, except for a kink around 1.75 mm. Since the THz amplitude grows linearly in the ideal
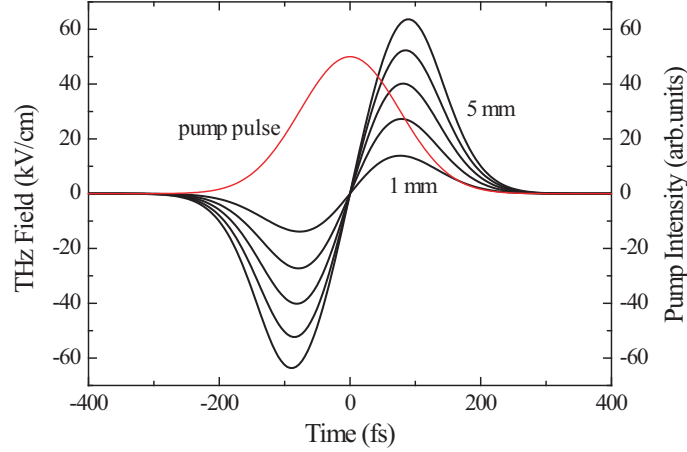
Fig. 6. Black lines: Temporal waveforms of THz field obtained under perfect phase matching and no absorption conditions. Red line: Temporal shape of the incident pump light pulse intensity.

case, as expressed in Eq. (17), this quadratic dependence is understood based on linear dependence of the speed of the red shifting or quadratic dependence of energy conversion efficiency on the THz field amplitude. In Fig. 2, it is seen that the central peak at 375 THz decreases and a red-shifted peak around 370 THz gradually grows in the propagation distance region between 0 and 2 mm. The height of the red-shifted peak exceeds around 1.75 mm, where the spectrum is not single-peaked. A blue-shifted peak is also seen to be generated at this distance, which is attributed to a sum frequency generation process. Propagation distance of 1.75 mm almost agrees with the cascading length of 1.76 mm. More blue-shifted peaks are generated at longer distances and they are also shifted to lower frquencies through propagation in the EO medium. The observation above on the simulation results shows that the cascading length, z_c, corresponds to a propagation distance where significant red shifting, change in the main peak shape, and generation of a blue-shifted peak occur in the spectrum of the pump pulses. These are regarded as the features showing that cascaded OR processes start to occur.

Interestingly, growth of the THz spectrum is influenced little by these changes in the optical spectrum. The initial THz spectrum shape is determined only by the pump pulse width in the case of $\Delta k = 0$ and $\alpha = 0$. Change in the spectrum shape during propagation is small, and the amplitude grows almost linearly. We plot the peak field of the THz pulse in time domain as a function of propagation distance in Fig. 4. The red straight line in the figure shows the result obtained using Eq. (17), which assumes that the pump light field does not change during propagation. The dependence shown in the figure is almost linear even at propagation distances larger than z_c. Below z_c, the simulation result almost overlaps with that of the linear dependence calculated from Eq. (17), and at and above z_c, small deviation from the linear dependence is seen while qualitative changes as seen in the optical waves shown in Figs. 2(b) and 3 are not observed.

In Fig. 5, we plot the photon conversion ratio, r_p, as calculated using Eq. (22). We observe a smooth quadratic growth, and r_p reaches seven times the Manley-Rowe limit at a propagation distance of 5 mm. Energy conversion efficiency, r_E, was 3.5% at this distance. Temporal waveforms of the THz pulses are plotted in Fig. 6. They show waveforms almost propartional to the time derivative of the pump pulse shape, as expressed in Eq. (18), and linear dependence of the amplitude on the propagation distance. Although the assumption of no change in the pump field
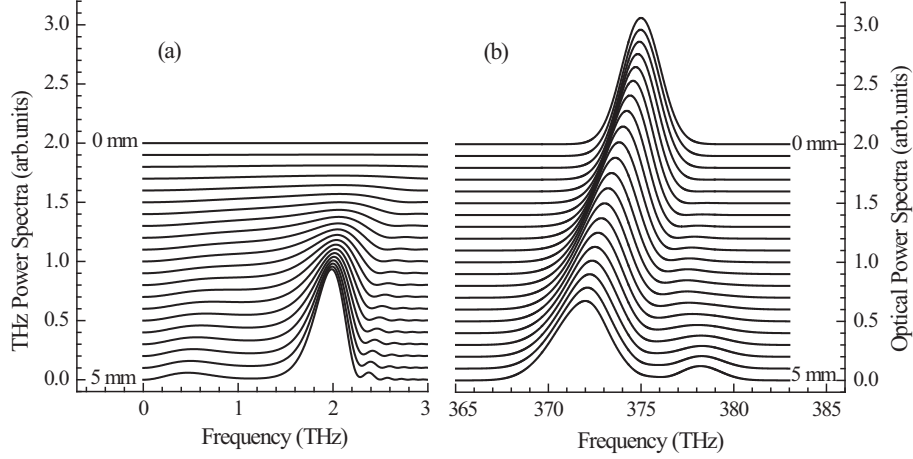
Fig. 7. Power spectra of (a) THz and (b) optical fields under realistic phase mismatches and no absorption conditions at propagation distances in the ZnTe crystal from 0 to 5 mm by a step of 0.25 mm. Each spectrum is shifted upward by 0.1.

is theoretically justified only in the limit of small conversion efficiency, the present results show that some predictions obtained using this assumption are valid even at conversion efficiencies higher than the Manley-Rowe limit.

3.2. $\Delta k \neq 0$, $\alpha = 0$ case

Now we examine the effects of phase mismatches on the cascaded OR processes by taking into account of finite phase mismatches, Δk_L and Δk_T. We keep the absorption at zero at this stage. Parameters of the pump pulses are the same as in the previous case. THz and optical spectra obtained by simulations are shown in Fig. 7 as a function of propagation distance. The peak of the THz spectra grows almost linearly, but the spectrum width becomes narrower as the propagation distance increases due to the phase matching condtion. The optical spectrum shows red shifting but the speed of the shift is much smaller than the perfectly phase matched case. Small shift of the peak frequency of the THz spectrum is observed. This is attributed to the shift in the THz frequency satisfying the phase matching condition because of the red shifting of the pump spectrum.

Temporal waveforms of the THz pulses are plotted in Fig. 8. The horizontal axis of the figure shows the local time traveling at the group velocity of the pump light. Spectral narrowing during propagation is clearly seen. Peak field in time domain grows up to a propagation distance of 2 mm. After that point, the peak field does not grow but the spectrum height grows because the pulse duration becomes longer and the spectrum is narrowed. Photon conversion ratio is plotted in Fig. 9. Photon conversion ratio larger than unity is obtained and there are no spurious behaviors at the crossover of $r_p = 1$.

The simulation results of this case shows that because of the dispersion of the EO medium, the phase matching condition can have a significant effect on the cascaded OR processes for THz pulse generation.

3.3. $\Delta k \neq 0$, $\alpha \neq 0$ case

Finite absorption coefficients of $\alpha_T = 12$ cm^{-1} and $\alpha_L = 3$ cm^{-1} are also included in the simulations now. In Fig. 10(a) and (b), we show the THz and optical spectra at the pump intensity same as that of the previous case of 300 MW/cm^2. Results obtained at a larger pump intensity
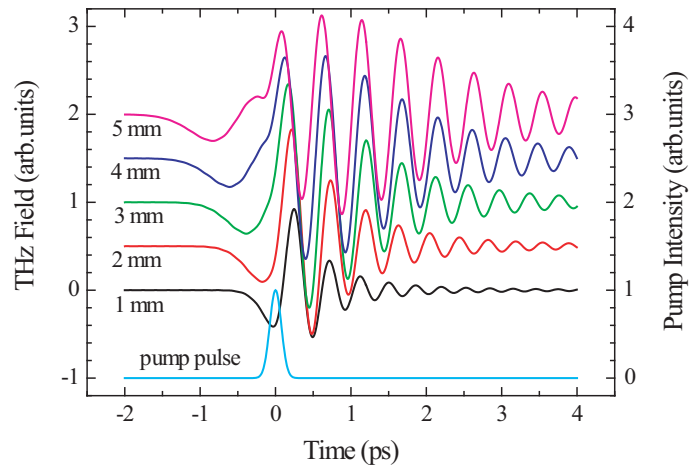
Fig. 8. Temporal waveforms of THz pulses obtained under realistic phase mismatches and no absorption conditions. Temporal shape of the incident pump pulse intensity is also shown.
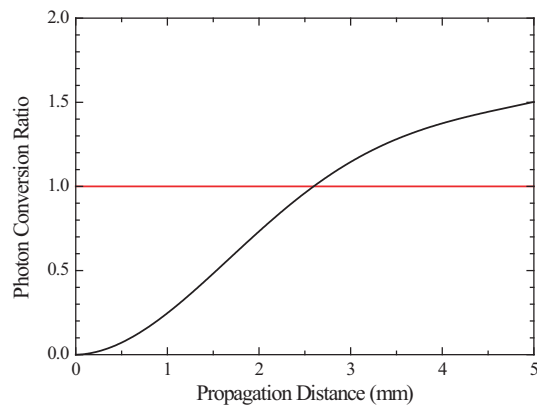

Fig. 9. Photon conversion ratio obtained under realistic phase mismatches and no absorption conditions. Red line shows the level of unity, which corresponds to the Manley-Rowe limit.
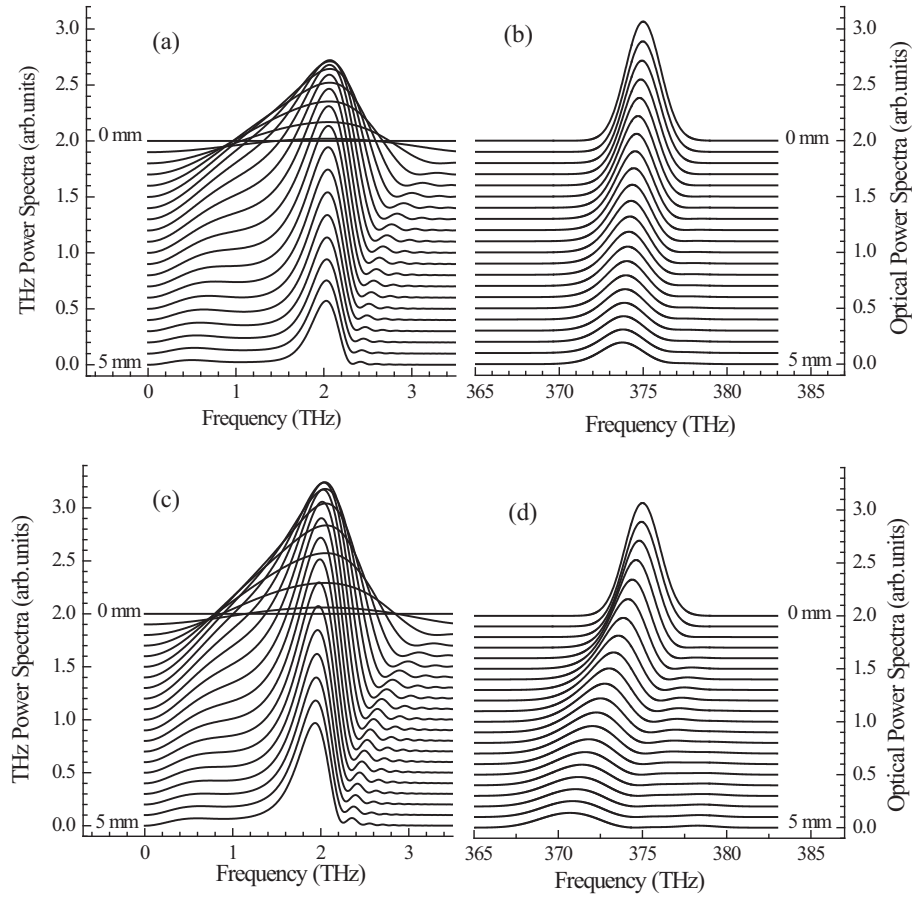
Fig. 10. Power spectra of THz and optical fields under realistic phase mismatches and absorption at propagation distances in the ZnTe crystal from 0 to 5 mm by a step of 0.25 mm. Each spectrum is shifted upward by 0.1. (a) THz spectra at 300 MW/cm^2 pump; (b) optical spectra at 300 MW/cm^2 pump; (c) THz spectra at 800 MW/cm^2 pump; and (d) optical spectra at 800 MW/cm^2 pump.
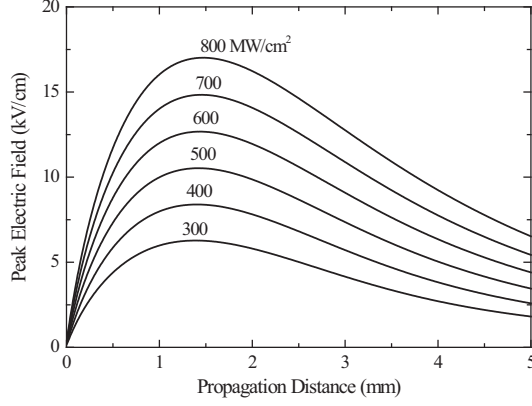
Fig. 11. Propagation distance dependence of the peak field of the THz temporal waveform at pump intensities of 300 to 800 MW/cm^2.

of 800 MW/cm^2 are shown in Fig. 10(c) and (d). In both cases, the THz spectra become maximum at a propagation distance of 2.25 mm, which agrees with $z_a = 2.3$ mm obtained using Eq. (28). Narrowing of the THz spectra is observed as seen in Fig. 7. Optical spectra show small red shift at 300 MW/cm^2 pump intensity. At 800 MW/cm^2, a significant red shift is observed. These results show that there is a competition between the nonlinear interaction and linear absorption of THz and optical fields, and cascaded OR processes occur at a high enough pump intensity.

In Fig. 11 is plotted the peak field of the THz temporal waveform as a function of propagation distance at incident pump intensities of 300 to 800 MW/cm^2. The field depends on the pump intensity almost linearly. The peak field is maximized at a propagation distance around 1.5 mm at all pump intensities. This is shorter than the propagation distance of 2.25 mm, where the THz spectrum reaches the maximum. This fact can be explained as follows. At the THz frequency where the phase matching condition is satisfied, the propagation behavior depends only on the absorption, thus the optimum distance agrees with z_a. In time domain, in contrast, the THz waveform is affected by both the phase matching and absorption. As seen in Fig. 8, growth of peak height in time domain is suppressed by the spectral narrowing due to phase matching condition. Thus the optimum propagation distance for the peak field in time domain is less than that for the spectrum peak.

3.4. Effects of pump pulse shape

As seen in the previous subsection, higher pump intensity increase the efficiency of THz pulse generation via cascaded OR processes. In actual experiments, however, two-photon absorption, which is not included in the present simulation model, increases at higher pump intensities. Consequently, methods to obtain larger THz amplitudes at less pump intensities are required. We study here effects of the pump pulse width and multiple pulse pumping.

Pump pulse width dependence of the power spectra of generated THz waves are calculated using Eq. (17), which is obtained under perfect phase matching and no loss conditions. Results are plotted in Fig. 12 for pulse widths from 100 to 300 fs. Peak incident intensity was kept constant in the calculations. It is seen from the figure that spectrum peak heights do not depend much on pump pulse width, and that peak frequencies and widths are in inverse proportion to pump pulse width. This can be explained by the fact that the influence of the pump pulse width comes from the integral in Eq. (17), which is the autocorrelation of the pump spectrum. When
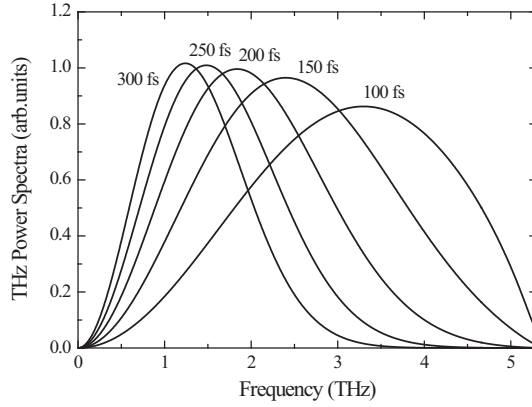
Fig. 12. Pulse width dependence of the THz power spectra under perfect phase matching and no loss conditions.
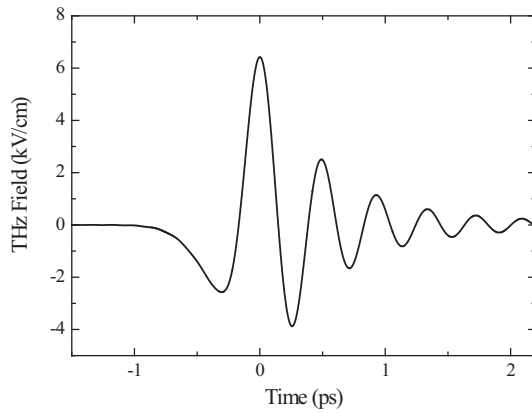

Fig. 13. Temporal waveform of THz pulse obtained at 1.66 mm when pumped by a 180 fs single pulse. Time zero is set at the peak time.

phase matching effects are taken into account, the THz spectrum should become narrower and be centered at 2 THz, where the phase matching condition is satisfied. The optimum pump pulse width that gives maximum THz output is about 200 fs, as seen from the figure. From calculations under the realistic phase mismatches and absorption conditions, it was found that the optimum pulse width depends on what quantity should be maximized. Time-domain peak field of the THz pulse was maximized at pump pulse width of 225 fs, and photon conversion ratio at 170 fs.

By pumping the EO medium using multiple pulses, we can obtain larger THz wave amplitudes while avoiding undisirable nonlinear effects such as two-photon absorption. Effects of multiple pulse pumping were investigated by examining the temporal peak field of THz pulse at a propagation distance of 1.66 mm, where the peak field was maximum. Incident pump intensity and pulse width were set at 300 MW/cm^2 and 180 fs. Effects of phase mismatches and absorption were included in the calculations. In Fig. 13 is shown the waveform of THz pulses obtained when pumped by a single pump pulse. After the main peak at time zero, peaks with less amplitudes are observed at 0.50, 0.93, 1.34, and 1.72 ps. THz waveforms obtained by multiple pulse pumping are expected to be time-shifted summations of this waveform. The op-
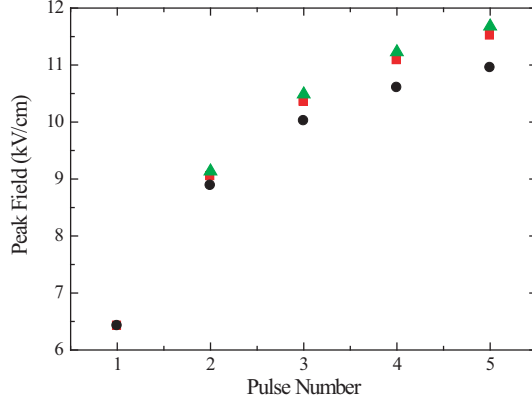
Fig. 14. Peak THz field obtained by multiple pulse pumping. Black circles and green triangles show results obtained by pumping with in-phase and out-of-phase pulse trains, respectively. Red squares are summations of peaks of the THz waveform obtained by single pulse pumping.

timum delay times, therefore, of additional pump pulses should be -0.50, -0.93, -1.34, and -1.72 ps in this order. In the calculations, the electric field of the pump light was expressed as a summation of time-shifted replicas of the original pulse shape. Peak intensity and pulse width for each pulse were kept at 300 MW/cm^2 and 180 fs.

Obtained peak THz fields are plotted in Fig. 14. Since there are overlaps between adjacent pump pulses, obtained THz peak fields depended on the relative phase of pump pulses. When phases of adjacent pump pulses are inverted, pump light intensity in the time region between the pulses become small because of destructive interference, and maximum THz output was obtained. The peak THz fields obtained by time-shifted summation of the waveform of single-pulse pumping case, as shown in Fig. 13, were between those obtained by in-phase and out-of-phase multiple-pulse pumping. Since the height of peaks in the trailing part of the THz waveform becomes less and less, effects of multiple pulse pumping on attainable peak field in time domain are limited, and maximum peak field of less than twice of that of single pulse pumping case was obtained at five pump pulses.

Effects of multiple pulse pumping on THz spectra are more pronounced. In Fig. 15, we plot temporal waveforms and power spectra of THz pulses obtained by one to five pump pulses. Fields of all the pump pulses were set to have the same phase in the calculations. It is seen from the figure that by multiple pulse pumping, the spectrum is narrowed to a peak frequency of 2.1 THz, and the enhancement in spectrum peak is more than 18 times from one to five pump pulses. The results show that multiple pulse pumping is very effective if large intensity of THz waves at a specific frequency is required.

4. Conclusion

We have conducted mumerical simulations based on one-dimensional coupled propagation equations of optical and THz waves for intense THz pulse generation using optical rectification in EO crystals. Effects of cascaded optical rectification processes are examined under perfect phase matching and no loss case and also under realistic phase matching or absorption conditions using parameters of ZnTe. Under ideal conditions, conversion efficiencies much higher than the Manley-Rowe limit were observed. Competition between cascaded optical rectifications and absorption was shown to be expressed in terms of characteristic lengths describing
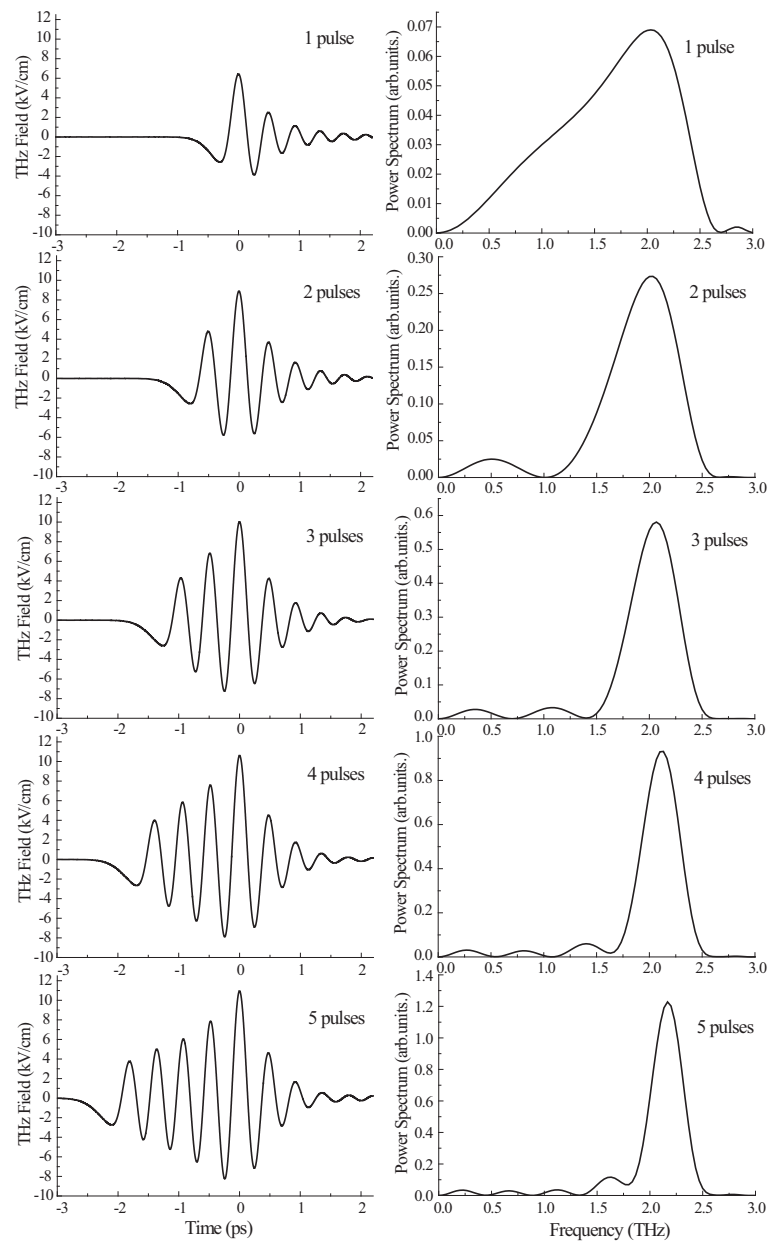
Fig. 15. Waveforms and power spectra of THz pulses obtained by multiple pulse pumping.

these effects. Red shifting of the pump light spectrum has been observed which exhibits the occurrence of cascaded processes. Effects of pump pulse width and multiple pulse pumping also have been studied.

Acknowledgments